Quantifying the vibrothermographic effect

Stephen D. Holland[a], Christopher Uhl[b], Zhong Ouyang[c], Tom Bantel[d], Ming Li[e], William Q. Meeker[e], John Lively[c], Lisa Brasche[f], David Eisenmann[f]

[a] *Center for NDE and Department of Aerospace Engineering, Iowa State University*
[b] *GE Aviation*
[c] *Pratt and Whitney*
[d] *GE Aviation (retired)*
[e] *Center for NDE and Department of Statistics, Iowa State University*
[f] *Center for NDE, Iowa State University*

Abstract

Vibrothermography, also known as Sonic IR and thermosonics, is a method for finding cracks through thermal imaging of vibration-induced crack heating. Due to large experimental variability and equipment which has, up to now, yielded mostly qualitative results, little data has been available to help quantify the vibrothermographic effect. This paper quantitatively evaluates the relationship between vibrothermographic crack heating, crack size, and vibrational stress in a series of tests on 63 specimens each of Ti-6-4 Titanium and Inconel 718 at three different sites with different equipment. Test specimens are excited in a resonant mode. Infrared cameras record the crack heating, and vibrational stress is evaluated from the known vibrational mode shape combined with vibrational velocities measured using a laser vibrometer. Crack heating increases both with crack length and dynamic vibrational stress level. Data from all three sites give similar probability of detection (POD) curves. The relationship of crack heating to crack size and vibrational stress will provide a means in the future to predict crack detectability based on vibration measurements

Key words: Vibrothermography, Sonic IR, Sonic Infrared, Thermosonics, crack heating, vibration

DOI: `http://dx.doi.org/10.1016/j.ndteint.2011.07.006`

Email address: `sdh4@iastate.edu` (Stephen D. Holland)

1. Introduction

The technique of vibrothermographic nondestructive inspection, also known as "sonic infrared" and "thermosonics" has been troubled by questions of reproducibility[1]. Vibrothermography involves exposing a crack to sonic or ultrasonic vibration, then observing induced heating with an infrared camera [2]. The mechanism of vibrothermographic heating of delaminations in composite materials has been investigated relatively thoroughly[3, 4], and observed data is generally consistent with a friction mechanism.

For metals, there is still substantial debate over the relative significance of friction versus other mechanisms such as plastic deformation [5]. Some numerical simulations suggest that plastic deformation is significant [6] and others suggest it is not [7]. In our own experiments the locus of heating is usually observed well inward (e.g. [8]) from the crack tips, consistent with a frictional theory but not with plastic deformation. Crack face deformation, observed with electron and optical microscopy, is seen at the heating zones away from the crack tips [9].

While vibrothermography has shown substantial promise for finding cracks in metals, to date no quantitative relation has been shown between vibrothermographic heating and key characteristics of the crack such as length or morphology. While some cracks can heat by several degrees, others heat little or not at all [10]. Theories of frictional heating have inspired simulations [11], but little quantitative experimental data has been available to validate those theories, in part because of the large amount of experimental variability. Lu et al. [12] showed a relation albeit in arbitrary units, between an energy metric related to relative motion across the crack and observed heating. One particularly notable result has been the work of Morbidini and Cawley [1], who developed a method for quantitatively predicting vibrothermographic heating from independent measurements of crack-induced damping, and then compared experimentally observed heating with those predictions.

A key prerequisite to widespread industrial deployment of vibrothermography is the ability to predict and quantify the performance of the inspection. Because the vibration is usually applied at frequencies on the same order as natural resonances, vibrothermographic crack detection performance is a strong function of both the overall shape of the specimen and the location of the crack within the pattern of resonances. Moreover, traditional synthetic defects such as electro discharge machining (EDM) notches and flat-bottom

holes do not generate vibrothermographic indications because they have no rubbing surfaces. A rigorous probability of detection (POD) study would require a large number of real, cracked specimens with cracks in a broad variety of locations for each type of part. In most applications such a study would be prohibitively expensive. A more viable alternative is to predict the reliability of the vibrothermographic test through relating the local vibration in the vicinity of the crack (or the vibration's statistics) with known dependence of crack heating on vibration. There have been previous large-scale investigations of parameter sensitivity [13] and POD [14], but without a way to quantify the physical stimulus the crack was exposed to, there is no clear way to extrapolate these results beyond the specific geometries involved.

In this paper we present quantitative experimental data relating crack heating to local longitudinal (crack opening/closing) vibration in a large specimen set. The data shows how much crack heating was observed for cracks of different lengths exposed to different levels of mode I vibrational stress. Testing was performed on two materials, Ti-6Al-4V Titanium and Inconel 718, and at three sites, Iowa State University (ISU), Pratt and Whitney (PW), and General Electric (GE). Despite substantial differences in excitation and measurement systems at the three sites, we observe the same relationship between vibrational stress, crack length, and crack heating.

2. Vibrothermographic testing

A vibrothermographic test typically involves a vibration source to excite the specimen, an infrared camera to observe heating of the flaw, and often a laser Doppler vibrometer to monitor the vibration amplitude. The vibration source, usually an ultrasonic welder, is pneumatically pressed to the sample, which is mounted using either a rigid or a compliant clamp. A coupling medium, such as paper, plastic, or cardstock separates the tip of the vibration source from the specimen. The vibrational excitation is typically activated for 1-2 seconds causing the crack surfaces to rub, generating heat which diffuses outwards. A computer records and processes the infrared images of the surface temperature profile along with the measured Doppler velocities from the laser vibrometer.

Since the vibrational wavelengths involved are on the order of the size of the specimens, resonances and resonance effects dominate the vibration. The ultrasonic welders commonly used as vibration sources can generate 1-2 kW of vibrational power at a fixed frequency such as 20 kHz. The 20

kHz pump frequency rarely coincides with a natural resonance and the mechanical impedance of the welder rarely matches that of the specimen. The welder tip is pressed to the specimen, but this connection does not support tension and is therefore nonlinear. The result of the extreme power level, mismatched impedance, and nonlinear interface is a hammering effect between tip and specimen that can generate a broad range of frequencies including harmonics and subharmonics some of which inevitably excite resonances of the specimen. The tip-specimen nonlinearity converts the single frequency vibration of the welder into the particular resonant frequencies of the specimen. Unfortunately, the relationship between excited resonances and the experimental configuration is so complicated as to defy analysis. The resonant spectrum of the specimen is a sensitive function of geometry and clamping parameters (boundary conditions). The precise transduction of energy from the 20 kHz pump frequency into specimen resonances is a geometry- and clamping-dependent nonlinear process that is difficult to repeat and may even be chaotic [15].

In these experiments we tuned the specimens to resonate in their 3rd order flexural (bending) mode at approximately 20 kHz. The 20 kHz excitation frequency is supported by the measurement systems at all three locations, ISU, PW, and GE. The tuned specimens naturally vibrate near the excitation frequency, minimizing the nonlinear hammering effect and the presence of other frequencies. Since the resonant mode shape is known it is possible to calculate the motion everywhere in the specimen from the motion at a single point, such as can be measured with a laser vibrometer. The tuned specimens and resonant vibrations mean that the experiments described here are far more controlled than in the typical vibrothermography experiment. Motion is, for the most part, at a single frequency and a single resonant mode. From the mode shape, frequency, and motion measured at a single point the vibrational stresses at the crack can be calculated so as to directly relate those stresses to observed heating.

3. Modeling

The most commonly hypothesized mechanism of crack heating is frictional rubbing between crack surfaces. In a frictional model, crack heating power P comes from sliding friction between contacting asperities. The amount of heating is the sum of the frictional energy of each asperity i, which depends on the relative velocity v_i and the static and dynamic normal forces N_i^s and

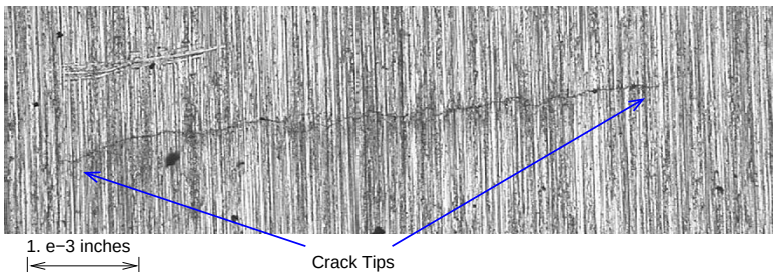

Figure 1: Visible white light image of a crack in titanium (sample #05-451)

N_i^d between the asperities respectively,

$$P = \sum_i \mu_i \ (N_i^s + N_i^d) \ |v_i| \ u(N_i^s + N_i^d) \tag{1}$$

where μ_i is the coefficient of friction of a particular asperity and $u(N)$ is the unit step function representing the lack of friction once normal force becomes negative. It might seem that heating would be largely proportional to shear, based on shear-induced frictional sliding. Rather, it is the *local* shearing motion that is significant. Cracks, such as that pictured in Fig. 1, are so irregular that even a pure opening or closing force will give rise to a substantial local shearing force on an angled surface. Substantial friction is possible even in an opening/closing mode.

Eq. 1 can be used to predict the relationship between crack heating and vibrational stress. Both dynamic normal force N_i^d and velocity v_i, through linearity of the stress-strain relation, are proportional to the dynamic vibrational stress at the part. The model of Eq. 1 therefore gives rise to a linear relationship between vibration and crack heating when static normal force dominates dynamic normal force, and a quadratic relationship when dynamic normal force dominates static normal force.

The relationship between crack length and crack heating is more difficult to predict. We would expect the amount of energy transformed into heat to be proportional to the rubbing surface area S, which we would assume to be the surface area of the the crack, S $\propto$ (length)^2 for half-penny cracks such as the ones tested here. In fact, it is clear from measurements of larger cracks, e.g. [8] that in some cases the actual heating zone may be just a thin semicircle rather than an entire crack face, giving S $\propto$ (length) instead. The relative mobility M between crack faces is also determined in part by crack

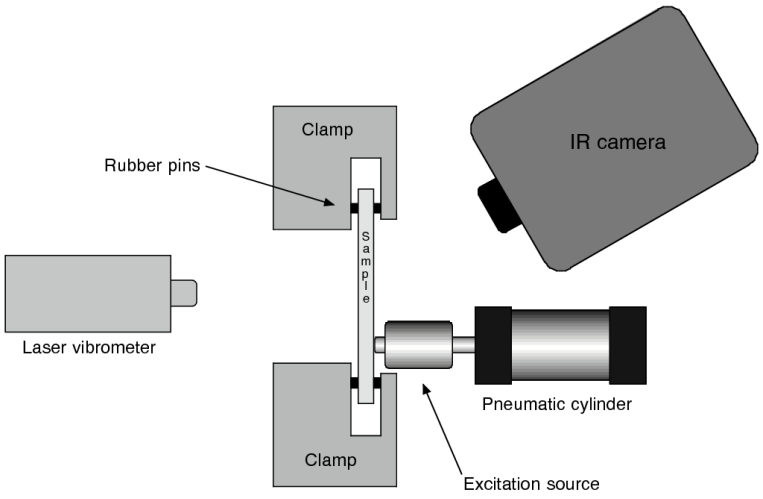

Figure 2: Common experimental configuration

length. Mobility between faces is highest at the crack center and zero at the tips. Based on the heating energy and temperature increase coming from mobility M $\times$ area S, where M $\propto$ (length) and S $\propto$ (length) or (length)^2, we would expect the temperature increase ΔT to be proportional to (length)^2 or (length)^3.

Note that we do not take into account the fact that for longer cracks, the heating zone observed on the surface would would be spread over that longer length, reducing the observed temperature and leading to a weaker length dependence than predicted above. We leave this out because for almost all the cracks used in these tests, the crack length was less than the characteristic thermal diffusion length so the size of the heating zone on the surface was essentially independent of crack length.

4. Measurement

A common experimental geometry, illustrated in Fig. 2, was used at all three sites[1]. A vibration source located off-center excites motion in the spec-

[1]Details of the geometry varied slightly between the sites. For example, the apparatus at ISU and PW was oriented horizontally as seen in the figure, whereas the apparatus

imen from the front (crack side). The specimen is mounted using rubber pins. A laser vibrometer records motion directly behind the crack, while an infrared camera images crack heating.

The Iowa State University (ISU) measurement system used in these tests uses a piezoelectric stack mounted to a pneumatic cylinder as a vibration source. The piezoelectric stack is driven by an arbitrary waveform generator and power amplifier. A FLIR SC6000 InSb cooled infrared camera captures images and a Polytec OFV-5000/OFV-505 laser vibrometer is used to measure specimen vibration. The arbitrary waveform capability and comparatively broadband piezoelectric stack give the ISU system the flexibility to excite over a wide range of frequencies, roughly 500 Hz to 30 kHz.

The Pratt and Whitney (PW) system uses a Branson 2000ea (2.2 kW rated power) ultrasonic welder mounted to a custom pneumatic cylinder assembly as a vibration source, a FLIR Phoenix InSb cooled infrared camera and a Polytec OFV-353/OFV 3001 laser vibrometer to monitor vibration. The General Electric (GE) system uses a Branson 921ae (2.0 kW rated power) welder assembly, a FLIR Phoenix InSb IR camera, and a Polytec OFV-503/OFV 5000 laser vibrometer. The ultrasonic welders of the PW and GE systems are limited to a single vibration frequency, roughly 20 KHz, but have a much higher power level capability than the broadband system at ISU.

The test specimens were a series of 63 Ti-6Al-4V and 63 Inconel 718 bars with preexisting half-penny shaped surface cracks. The cracks were originally created through cyclic fatigue (R=0.1) in three point bending to a maximum stress of 80% of yield. The cracks were initiated using electro-discharge-machining (EDM) notches that were later machined away. The specimen geometry is shown in Fig. 3. All specimens were tuned through length adjustment to have third order flexural resonant frequencies of approximately 20 kHz.

In the third order flexural resonance, vibrational stresses can be readily calculated from theory. Bending stresses at the symmetry point on the

---

at GE was oriented vertically, with the laser vibrometer reflected off a mirror under the specimen. The GE apparatus was also mirror-imaged relative to ISU and PW. In addition the laser vibrometer measurement at PW was at a slight angle, whereas normal incidence was used at ISU and GE.

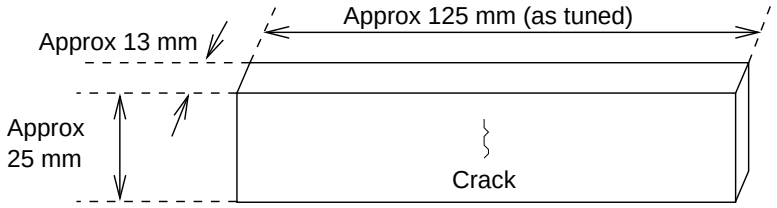

Figure 3: Specimen geometry:

surface of an odd-order (symmetric) flexural resonance are (via [16])

$$\sigma_{xx} = \frac{Eh}{2}\kappa^2 \left(\frac{\cosh \kappa L/2 - \cos \kappa L/2}{\cos \kappa L/2 + \cosh \kappa L/2} \right) z, \tag{2}$$

for modulus E specimen thickness h, length L, and central displacement z. In the third order flexural resonance used here the wavenumber $\kappa = 10.996/L$, thus

$$\sigma_{xx} = 59.760 \frac{Eh}{L^2} z. \tag{3}$$

For harmonic motion, the stress amplitude σ_{xx} in terms of velocity amplitude $\dot{z}$ is

$$\sigma_{xx} = 59.760 \frac{Eh}{2\pi i f L^2} \dot{z}, \tag{4}$$

where f is frequency and the imaginary number i is a reminder of the 90° phase shift between velocity and stress. In this way we calculate dynamic vibrational stresses σ_{xx} from the velocities $\dot{z}$ measured with the laser vibrometer.

5. Experiment

Specimen preparation began at ISU with the specimen tuning process and a cleaning/painting process to ensure good infrared emissivity. Each specimen was cut shorter to move its third order flexural resonance to a target frequency of 20.07 kHz, based on its geometry and observed resonant frequency. The resulting tuned specimens had the distributions of resonant frequency shown in Fig. 4 for titanium and Inconel. Laser vibrometry scans [10] were used to verify that the mode shape matched those predicted by flexural wave theory.

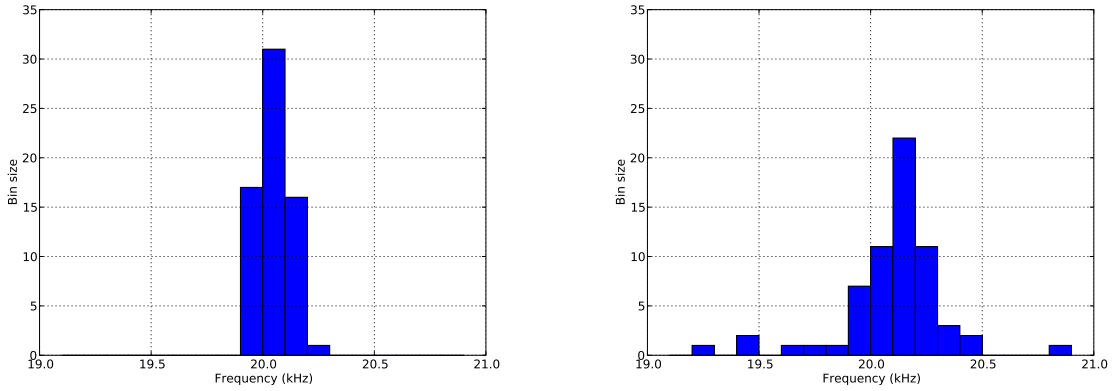

(a) (b)

Figure 4: Histograms of measured resonant frequencies of (a) tuned titanium specimens (b) tuned Inconel specimens.

At ISU the measurements on each sample began with a .2-25 kHz frequency sweep to determine the actual resonant frequency of the specimen. The sample measurements continued with two 1-second tests at each of three amplitude settings (0.5V, 1V, and 1.5V), performed in randomized order. One of the two tests was excited at the measured resonant frequency, and the other was excited at the nominal target resonant frequency of 20.07 kHz. The other two sites, PW and GE each did six 2-second tests per sample, at three amplitude settings (20%, 30%, and 40% of maximum) in randomized order at approximately 20 kHz. The infrared data from all the sites was temperature calibrated and stored along with the vibrometry data in a common format.

The measured infrared sequences and vibrometry waveforms were analyzed so as to develop a meaningful relation between dynamic vibrational stress and heating. Infrared data was taken from a single frame, one second after excitation start, making the longer excitations used at PW and GE irrelevant. The averaged background was subtracted from this frame[2]. Some

[2]Due to an error during data collection, some of the PW infrared sequences lacked background images taken before the excitation was turned on. In this case background images from well after the excitation was turned off were used for the background subtraction. The spatial high-pass filtering made this irrelevant.

of the infrared sequences showed nonstationary behavior such as very high power blooms as the excitation turned on. After these blooms, both the heating and vibration stabilized for the remainder of the test in almost all cases. To reduce the influence of transient behavior such as these blooms, the background-subtracted infrared image was spatially high-pass filtered, eliminating them. To estimate the heating temperature, a two-dimensional elliptical Gaussian profile was fit to the observed heating. The heating temperature was taken to be 0.95 times the peak of the Gaussian, with the 0.95 factor arbitrarily selected to be consistent with manual estimates of crack heating based on the same images. It represents the average temperature over the top 20% of the Gaussian and is a more representative temperature than the very peak.

Dynamic vibrational stresses were calculated from the measured vibrometry data. The laser vibrometer directly measures surface velocity $\dot{z}$ in m/s as a function of time. Waveforms consisted of an initial transient (the power blooms discussed above), followed by a strong and consistent oscillation at the excitation frequency plus weaker harmonics. The measured velocity waveform was cut into one period segments and the maximum and minimum velocities were subtracted to yield a peak-to-peak velocity in that segment. We applied Eq. 4 to evaluate the corresponding peak-to-peak vibrational stress. To minimize the effect of anomalous bursts of vibration such as the aforementioned power blooms, the median of the peak-to-peak stresses was used to represent the typical dynamic stress for an experiment. The calculated vibrational stresses are engineering stresses in that they do not include the reduction in cross section or stress concentration due to the crack itself.

The stress calculations are dependent on the assumption that Eq. 4 is valid even when the excitation frequency does not exactly match the specimen resonance, due to the distribution of resonant frequencies shown in Fig. 4. The validity of Eq. 4 was confirmed qualitatively in two ways: First, by observation through laser vibrometer scans that the mode shape does not change with small changes in frequency, and second, by verifying that the crack heating data acquired at ISU for excitation at the measured resonant frequency matched that for excitation at the nominal resonance of 20.07 kHz. Figure 5 shows plots, similar to those discussed below, of crack heating as a function of dynamic stress for excitations at nominal resonant frequency and for excitations at measured resonant frequency in titanium. Since the trends and heating values in Figs. 5a and 5b are similar except for the lower stress levels achieved off resonance, any variation in crack heating dependence

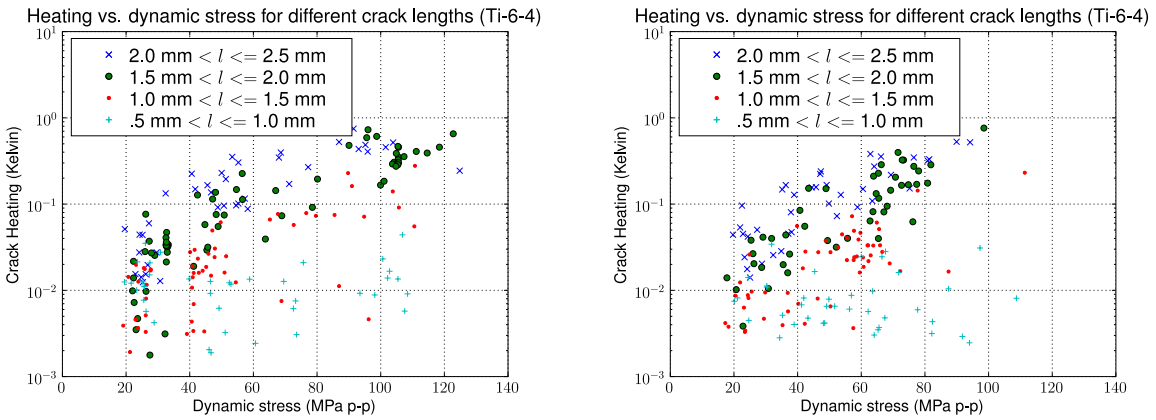

(a) (b)

Figure 5: Observed crack heating vs. dynamic vibrational stress, as measured at ISU using excitation (a) at resonant frequency of each specimen, and (b) at the nominal resonant frequency of 20.07 kHz.

from misestimation of dynamic stress from being off-resonance is likely small compared with the other sources of variation. Based on these validations we conclude that the calculated dynamic stress values are at least a reasonable approximation of the vibrational engineering stress applied to the specimen.

6. Results

Crack heating and vibrational dynamic stress data were collected for both the Titanium and Inconel specimen sets at ISU, PW, and GE, yielding a total of six data sets. Figures 6a and 6b show composite data from all three sites relating crack length to crack heating for the titanium and Inconel samples respectively. The data points are binned into four dynamic stress ranges. The distribution of crack lengths is nonuniform because the cracks were intentionally grown to a range of lengths. The higher stress level ranges correspond to more heating for a particular crack length. It is clear from the plot that longer cracks generally give more heating at a given stress level. The trend is consistent except for very low heating levels (< 40 mK) and for the longest cracks. At low heating levels the measured heating is dominated by infrared sensor noise, not by the actual amount of heating of the specimen. For the longest cracks, the length approaches the characteristic thermal diffusion length (2.8 mm for Ti-6-4 and 3.0 mm for Inconel 718).

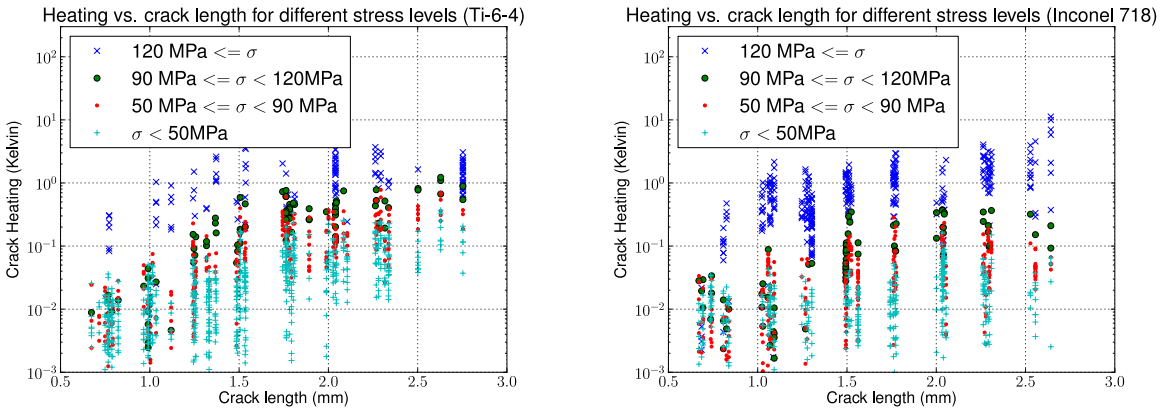

(a) (b)

Figure 6: Composite data from ISU, PW, and GE showing the observed relationship between crack heating and crack length in (a) Ti-6-4 and (b) Inconel 718. The data are binned according to applied dynamic vibrational stress level σ.

Thus the heating zone grows slightly with crack length for the longest cracks, the thermal energy is more spread out, and the overall temperature is slightly lower.

Because of the difference in capability between the measurement systems at the three sites, different regions within Fig. 6 are composed of data from different sites. Fig. 7 shows the composition of Fig. 6 from the constituent data gathered at ISU, PW, and GE. The results from each site follow the same trends of increasing heating with length and stress observed in the composite data set. Nevertheless, there are clear differences which result from the different vibrational excitation sources at the three sites.

The broadband piezoelectric stack-based ISU excitation system generated in general very low dynamic stress levels compared to those generated by the ultrasonic welder based PW and GE systems. Very few x's are seen in the ISU data of Fig. 7 representing the comparatively low stress levels achieved by the ISU system. The PW and GE systems commonly generated very high stress levels, and many x's are seen in the bottom two rows of Fig. 7. Likewise almost no heating values from ISU exceed 1 degree Kelvin (10^0), whereas many heating values from PW and GE exceed 1 degree Kelvin.

In three out of the four sets of experiments, the welder-based systems generated bimodal distributions of vibration (stress) amplitudes. Some tests generated very large vibrational stress amplitudes, whereas others generated

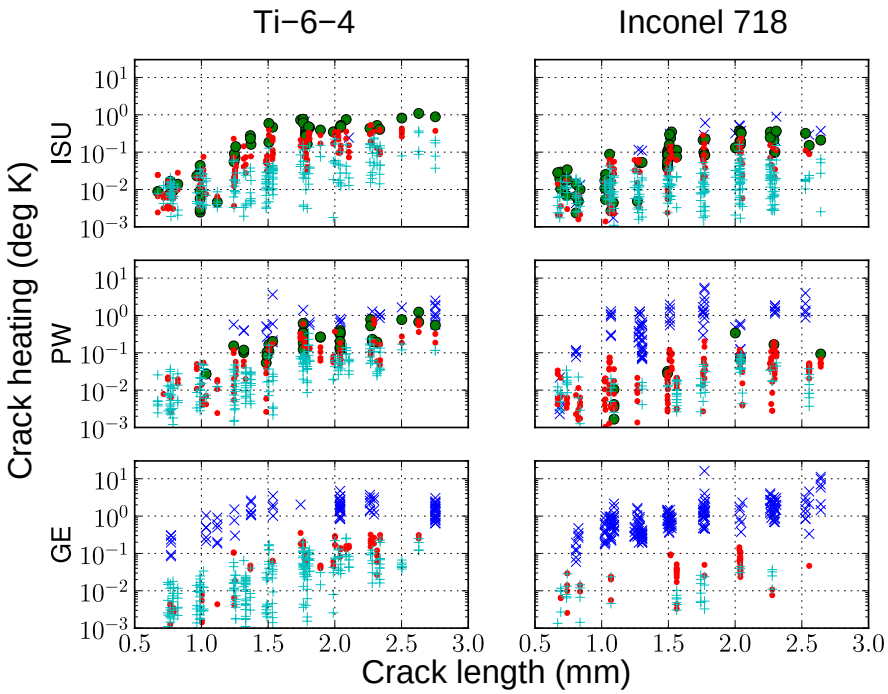

Figure 7: Constituent data of Fig. 6a (left) and Fig. 6b (right) from ISU, PW, and GE. Binning is the same as Fig. 6.

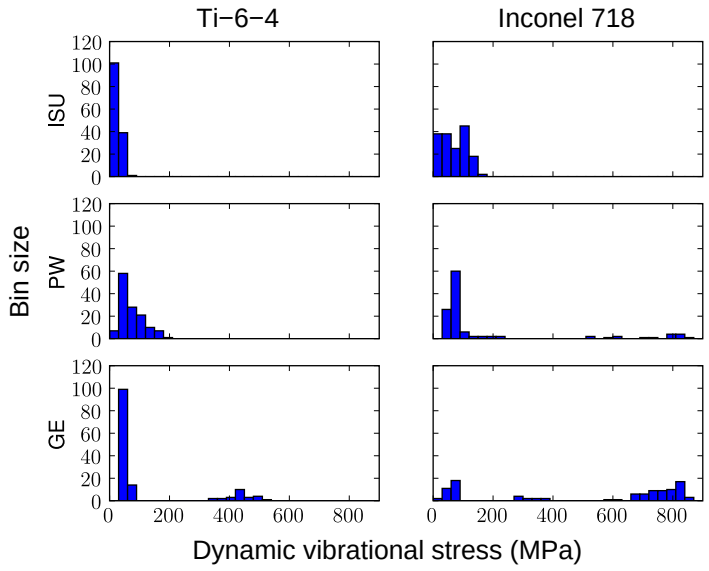

Figure 8: Histograms of dynamic stress amplitudes for each material at each site

very low amplitudes. These are seen in Fig. 7 as the lack of discs (stresses between 90 and 120 MPa) both in all the GE data and in the PW data for Inconel. Figure 8 shows histograms of achieved stress amplitudes for the maximum amplitude setting at ISU, PW, and GE. While most of the excitations at all sites achieved less than 200 MPa p-p vibrational stress, a percentage of the GE excitations along with a small number of the PW Inconel excitations achieved far higher vibrational stress levels, between 300 and 900 MPa p-p. The very high vibration amplitudes likely occurred when the resonant frequencies of the welder and specimen matched so closely as to allow the welder to deliver much more power than otherwise possible. This hypothesis is supported by a very strong correlation of very high vibrational amplitudes with observed resonant frequencies within a specific range (20.1-20.3 kHz).

A danger of the very high stress levels which might be achieved through resonance is the risk of fatigue damage or crack growth. It is well known [17] that fatigue processes can operate at acoustic or even ultrasonic frequencies. In this series of tests in 126 samples of two materials, crack growth was observed in exactly one specimen that was exposed to extraordinarily high stress levels, for an unusually high number of cycles. This Inconel spec-

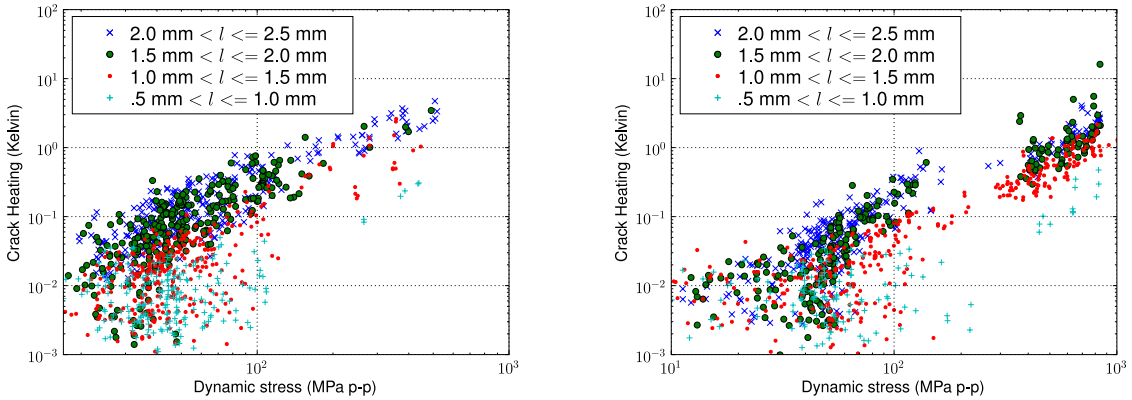

Figure 9: Composite data from ISU, PW, and GE showing observed crack heating vs. dynamic vibrational stress for several crack length ranges for (a) Ti-6-4, and (b) Inconel 718.

imen, with a preexisting crack and corresponding stress concentration, was exposed to fully reversing vibrational engineering stresses of approximately 800 MPa p-p (±400 MPa) – 38% of yield – for an estimated 160,000 cycles in addition to many more cycles at lower stress levels. The combination of resonant excitation, whether intentional or inadvertent, with high-power-capable ultrasonic welders and large numbers of tests should be avoided.

The very same crack heating data can also be plotted as a function of dynamic stress for different crack lengths, as shown in figures 9a and 9b. Looking at Figs. 6 and 9 we see that a crack in titanium at least 1.5 mm long exposed to 60 MPa p-p (±30 MPa) vibrational stress under the conditions of this test should be detectable with vibrothermography. Because heating is clearly tied both to crack length and stress level, a better way to evaluate detectability is through a *crack heating surface* or *crack detectability surface*: crack heating as a function of length and stress [10]. Such a surface fit based on a simple power law $\Delta T = c_1 l^{c_2} \sigma^{c_3}$ (neglecting the camera noise) is shown in fig 10. The surface is colored red beyond 50 mK, well above the detectability threshold of a modern IR camera and gray elsewhere. If the crack length and stress are within the red region then the crack should be detectable.

The crack heating surface is also useful because it provides a means to test the predictive capacity of models such as Eq. 1. Surface fits give $c_2 =$

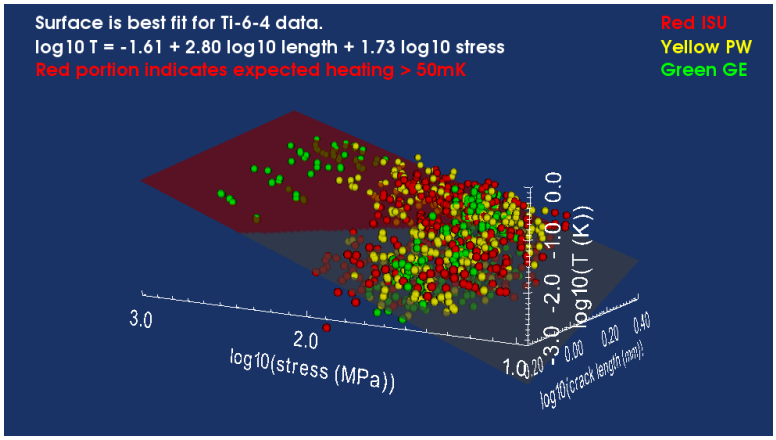

Figure 10: (Multimedia video online) Graphical animation of the crack detectability surface for titanium: Crack heating as a function of crack length and dynamic vibrational stress. Red data points come from ISU, yellow from PW, and green from GE. The semi-transparent surface fit is colored gray below the threshold of easy detectability (50 mK) and red above the threshold.

$2.8 \pm 0.2, c_3 = 1.73 \pm .06$ for titanium and $c_2 = 1.9 \pm 0.2, c_3 = 1.49 \pm .05$ for Inconel. The c_3 (stress power) values are consistent with the linear/quadratic prediction of Eq. 1. The c_2 (length power) value of 2.8 for titanium and 1.9 for Inconel are consistent with the $(\text{length})^2$ or $(\text{length})^3$ prediction mentioned in the discussion following Eq. 1.

With a heating surface model and a noise model it is possible to estimate probability of detection (POD) as a function of crack length for particular stress levels [18, 19]. This was done for the data for both materials from all three sites for a stress level of 100 MPa, as shown in Fig. 11.

The figure shows that each material gives similar POD curves for all three sites. The similarities between POD curves for the three sites verifies that all three sites are measuring essentially the same phenomenon despite substantial differences between measurement systems. It demonstrates cross-site reproducibility, a long standing problem in vibrothermography measurements.

7. Conclusions

This paper presents some of the first quantitative data relating vibrothermographic crack heating to local vibrational stress and crack length. While these results are directly applicable only to these particular cracks excited in

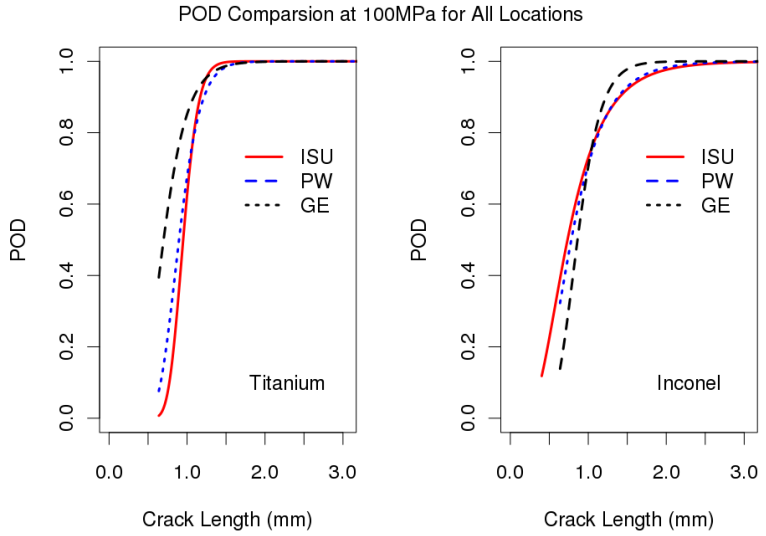

Figure 11: POD curves for 100 MPa p-p dynamic stress in titanium (left) and Inconel (right), based on separate ISU, PW, and GE measurements.

longitudinal (mode I) vibration at 20 kHz, they provide a useful data point for future estimation and prediction of crack detectability. The similarity of the results at Iowa State University, Pratt and Whitney, and GE Aviation show that despite what appears to be substantial innate variability, equivalent and comparable measurements can be performed with very different excitation and measurement systems. Combined with future methods for evaluating the dynamic stress fields in vibrothermographic tests of useful parts, knowledge of the relationship between vibrational stress and crack heating will provide the basis for predicting crack detectability in vibrothermography.

8. Acknowledgments

This material is based on work supported by the Federal Aviation Administration under Contract #DTFA03-98-D-00008, Delivery Order #0037 and performed at Iowa State University's Center for NDE as part of the Engine Titanium Consortium Phase III Thermal Acoustic Studies program.

References

[1] M. Morbidini, P. Cawley, T. Barden, D. Almond, and P. Duffour, Prediction of the thermosonic signal from fatigue cracks in metals using vibration damping measurements, J. Appl. Phys **100** 104905 (2006)

[2] X. Maldague, *Theory and Practice of Infrared Technology for Nondestructive Testing* , John Wiley and Sons, New York (2001).

[3] K. L. Reifsnider, E. G. Henneke, W. W. Stinchcomb, "The Mechanics of Vibrothermography", in *Mechanics of Nondestructive Testing*, ed. W. W. Stinchcomb (Plenum Press, New York) 249–276 (1980)

[4] A. Mian, X. Han, S. Islam, and G. Newaz, Fatigue damage detection in graphite/epoxy composites using sonic infrared imaging technique, Composites Science and Technology **64** 657–666 (2004)

[5] C. Homma, M. Rothenfusser, J. Baumann, and R. Shannon, Study of the heat generation mechanism in acoustic thermography, Review of Progress in Quantitative Nondestructive Evaluation **25** 566–573 (2006)

[6] F. Mabrouki, M. Thomas, M. Genest, and A. Fahr, Numerical modeling of vibrothermography based on plastic deformation NDT&E International **43** 476–483 (2010)

[7] X. Han, M.S. Islam, G. Newaz, L.D. Favro, and R.L. Thomas, Finite element modeling of the heating of cracks during sonic infrared imaging, J. Appl. Phys. **99** 074905 (2006).

[8] J. Renshaw, S. D. Holland, and R. B. Thompson, Measurement of crack opening stresses and crack closure stress profiles from heat generation in vibrating cracks, Appl. Phys. Lett **93** 081914 (2008)

[9] J. Renshaw, S. D. Holland, R. B. Thompson, and J. Anderegg, Vibration-induced tribological damage to fracture surfaces via vibrothermography, Int. J. Fatigue **33**(7) 849–857 (2011)

[10] S. D. Holland, C. Uhl, and J. Renshaw, Toward a viable strategy for estimating vibrothermographic probability of detection, Review of Progress in Quantitative Nondestructive Evaluation **27** 491–497 (2008).

[11] X. Han, A. S. Ajanahalli, Z. Ahmed, W. Li, G. M. Newaz, L. D. Favro, and R. L. Thomas, Finite-element modeling of sonic ir imaging of cracks in aluminum and titanium alloys, Review of Progress in Quantitative Nondestructive Evaluation **27** 483–490 (2008).

[12] J. Lu, X. Han, G. Newaz, L.D. Favro, and R.L. Thomas, Study of the effect of crack closure in sonic infrared imaging, Nondestructive Testing and Evaluation **22** 127–135 (2007)

[13] D. Mayton, F. Spencer, and C. Alvarez, Characterizing the effects of sonic ir variables on turbine disk inspection using a design of experiments approach, Review of Progress in Quantitative Nondestructive Evaluation **24** 642–649 (2005)

[14] J. DiMambro, D.M. Ashbaugh, C.L. Nelson, and F.W. Spencer, Sonic infrared (IR) imaging and fluorescent penetrant inspection probability of detection (POD) comparison, Review of Progress in Quantitative Nondestructive Evaluation **26** 463–470 (2007)

[15] X. Han, W. Li, Z. Zeng, L. D. Favro, and R. L. Thomas, Acoustic chaos and sonic infrared imaging, Appl. Phys. Lett. **81**(17) 3188–3190 (2002).

[16] W. C. Elmore and M. A. Heald, *Physics of Waves*, Dover Publications, pp. 114-122.

[17] E. J. Richards, and D. J. Mead, Noise and acoustic fatigue in aeronautics, Wiley 1968. Noise and acoustic fatigue in aeronautics

[18] M. Li and W. Q. Meeker, A noise interference model for estimating probability of detection for nondestructive evaluations, Review of Progress in Quantitative Nondestructive Evaluation 2008, AIP Conf. Proc. 1096 1769-1776 (2009).

[19] M. Li, S. D. Holland, W. Q. Meeker, Quantitative multi-inspection-site comparison of probability of detection for vibrothermography nondestructive evaluation data, Under review, Journal of Nondestructive Evaluation (2011)
Preprint: http://www.stat.iastate.edu/preprint/articles/2011-04.pdf